Indonesian Journal of Biotechnology

VOLUME 25(2), 2020, 102-108 | RESEARCH ARTICLE

Computational modeling of AGO-mediated molecular inhibition of ARF6 by miR-145

Jeremias Ivan[1], Rizky Nurdiansyah[1], Arli Aditya Parikesit[1,*]

Department of Bioinformatics, School of Life Sciences, Indonesia International Institute for Life Sciences, Pulomas Barat Kav 88, Jakarta Timur 13210, Indonesia

*Corresponding author: arli.parikesit@i3l.ac.id

SUBMITTED 23 April 2020 **REVISED** 29 June 2020 **ACCEPTED** 15 September 2020

ABSTRACT Inhibition of ADP-ribosylation factor 6 messenger RNA (ARF6 mRNA) by microRNA-145 (miR-145), mediated by Argonaute (AGO) protein, has been found to play essential roles in several types of cancer and cellular processes. This study aimed to model the molecular interaction between miR-145 and ARF6 mRNA with AGO protein. The sequences of miR-145 and the 3' untranslated region (UTR) of ARF6 mRNA were retrieved from miRTarBase, followed by miRNA target-site and structure predictions were done using RNAhybrid, RNAfold, and simRNAweb, respectively. The interaction between the miRNA-mRNA duplex and AGO was further assessed via molecular docking, interaction analysis, and dynamics, using PatchDock Server, PLIP, and VMD/NAMD, respectively. The models between miR-145, predicted target site of ARF6 mRNA, and AGO protein returned stable thermodynamic variables with negative free energy. Specifically, the RNA duplex had an energy of -19.80 kcal/mol, while the docking had -84.58 atomic contact energy supported by 70 hydrogen bonds and 14 hydrophobic interactions. However, the stability of the RMSD plot was still unclear due to limited computational resources. Nevertheless, these results computationally confirm favorable interaction of the three molecules, which can be utilized for further transcriptomics-based drugs or treatments.

KEYWORDS Gene silencing; in silico; molecular simulation; transcriptomics; tumorigenesis

1. Introduction

ADP ribosylation factor 6 (ARF6) is a small GTPase that plays a role in diverse cellular processes, including cell adhesion and migration (Li et al. 2018). Previous studies found that ARF6 acts as an oncogene, promoting tumor cell invasion in several cancer types (Hashimoto et al. 2004; Eades et al. 2015; Xu et al. 2019). According to Sabe (2003), the expression of ARF6 would inactivate the activity of E-cadherin, thus reducing the cell junctions. It is coupled with an increased N-cadherin expression, which allows the cells to attach to collagen, a component of extracellular matrix (Janiszewska et al. 2020). It also plays a role in the fibroblast growth factor receptor (FGFR) and Wnt signaling pathways (Mrozik et al. 2018). These processes allow the cells to move to the extracellular matrix, enter the lymphatic/blood systems, and extravasate to form tumors (Oh et al. 2012). ARF6 expression also correlates with other processes, such as macrophage-mediated inflammation (Li et al. 2018). The activity of ARF6 is post-transcriptionally regulated by tumor suppressor miR-145 (Zeinali et al. 2019) via the binding to the 3' UTR of the ARF6 mRNA (Pashaei et al. 2016). However, long non-coding RNA regulator of reprogramming (lincRNA-RoR) acts as a natural competitor or sponge for miR-145, inhibiting the miRNA activity (Eades et al. 2015). This would lead to the overexpression of ARF6 and eventually the formation of tumors.

RNA silencing process requires the presence of the RNA-Induced Silencing Complex (RISC), a ribonucleoprotein complex that utilizes small RNA as a template to recognize the complementary sequence of the target mRNA (Zhang 2013). One major constructor of RISC is Argonaute (AGO) protein (Zhang et al. 2018), which acts as an essential effector in post-transcriptional gene silencing (Li et al. 2014). Structurally, AGO protein consists of N-terminal, PAZ, MID, and PIWI domains, which are organized in a bilobal conformation (Djuranovic et al. 2011). Specifically, the PAZ domain would bind to the 3' end of the miRNA, while the 5' end would anchor to the MID domain (Li et al. 2014). The binding of miRNA to the AGO protein would 'guide' the AGO-centered RISC to bind with the complementary mRNA at 3' UTR region, leading to mRNA cleavage (Zhang 2013). As AGO protein plays an important role in RNA silencing, it is crucial to understand the molecular interaction between these three molecules. This can be modeled via molecular docking

simulation, which will be followed by molecular dynamics simulation to assess the stability of the molecules. By mimicking the condition of cytoplasm where the miRNA-mediated gene silencing process mainly occurs (Liu et al. 2018), we can computationally assess the behavior of the molecules in the real environment. In this study, the molecular simulations were done between AGO protein and miR145-ARF6 mRNA duplex, aiming to model the interaction based on in silico point of view for further development of drug and treatments.

2. Materials and Methods

In this study, the pipeline was constructed based on other similar studies (e.g. Das et al. (2015) and Rath et al. (2016)). Several adjustments were made to match the requirements of the software with the available computer resources. The complete pipeline is shown in Figure 1.

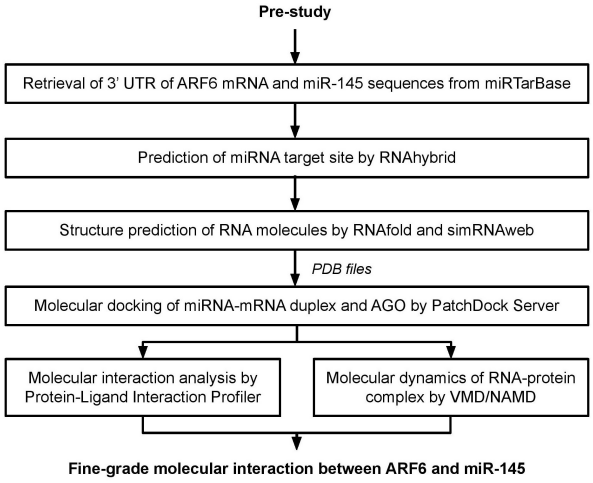

FIGURE 1 Pipeline of the study.

2.1. Sequence retrieval and structure prediction

The sequences of miR-145 and 3' UTR region of ARF6 mRNA were retrieved from miRTarBase under the 'miRNA' and 'Target Gene' tabs, respectively (accession ID: MIRT278608) (Chou et al. 2018). After that, the miRNA target site was predicted by using RNAhybrid (Rehmsmeier et al. 2004). The secondary and tertiary structures of miR-145, its predicted target site, and the miRNA-mRNA duplex were then visualized by using RNAfold (Lorenz et al. 2011) and simRNAweb (Boniecki et al. 2015; Magnus et al. 2016), respectively.

2.2. Molecular docking and dynamics

The miRNA molecule was blindly docked with human AGO-2 protein (PDB ID: 4F3T) to locate the binding site by using PatchDock Server (Duhovny et al. 2002; Schneidman-Duhovny et al. 2005), followed by the docking between the miRNA-mRNA duplex and the protein. PatchDock Server utilized rigid docking based on the geometries of the molecules (Schneidman-Duhovny et al. 2005). As a comparison, the protein was also docked with its native ligand (miR-20a) by using the same software. The molecular interaction between the protein-miRNA and protein-duplex was then assessed by using Protein-Ligand Interaction Profiler (PLIP) (Salentin et al. 2015).

Lastly, molecular dynamics of the complex were simulated by using VMD/NAMD pipeline under NVT condition (i.e. constant particle number, volume, and temperature) by following the NAMD Tutorial file (http://www.ks.uiuc.edu/Research/namd/) (Humphrey et al. 1996; Phillips et al. 2005). The complex was first solved into a water box, followed by energy minimization for 1,000 steps at 1 atm (pressure) and 310 K (temperature). The resulting coordinate files alongside the combination of protein, nucleotide, carbohydrate, lipid, water, and CHARMM general force fields were then used for the analysis with 1,650,000 steps. The CHARMM topology and parameter files were taken from MacKerell Jr (2001).

All analysis was done under default parameters of each software (Zhang and Verbeek 2010; Ahirwar et al. 2016; Lorenz et al. 2016; Magnus et al. 2016) in Windows computer with Intel® Core™ i7-8750H CPU @2.2GHz and 8GB RAM. The tertiary structures of the simulation were then visualized in the VMD tool and PyMOL (The PyMOL Molecular Graphics System, Version 2.3.0, Schrodinger, LLC), respectively. The 2D/3D structure prediction steps took around 14 days (depends on the online queue), while the molecular docking and dynamics required one and seven days, respectively.

3. Results and Discussion

3.1. Sequence retrieval and structure prediction

After the sequences of miR-145 and 3' UTR of ARF6 was retrieved from the miRTarBase, the miRNA target site was predicted using RNAhybrid. The predicted site turned to match the prediction by miRanda (Betel et al. 2008) that is stored in the miRTarBase entry (accession ID: MIRT278608); there is binding between ARF6 mRNA and miR-145 at the 956th position of the UTR region, denoted by 20 pairing nucleotides (Figure 2, yellow-highlighted areas). Nucleotide bindings are characterized by hydrogen bonds between A-U (two bonds) and C-G (three bonds) of the interacting nucleobases. Besides, the minimum free energy (MFE) of the binding is -28.2 kcal/mol, showing favorable interaction. However, the p-

```
3' UTR of ARF6   5' A  U  C        C          A 3'
                    AG GA UUUUGGG AAAACUGGA
                    UC CU AGGACCC UUUUGACCU
miR-145          3'   C  A                  G 5'
```

FIGURE 2 Prediction of the miR-145 binding site on 3' UTR of ARF6 mRNA. The second line is the part of the first line (ARF6) and the third line is the part of the fourth line (miR-145). The interacting nucleotides were placed near to each other and highlighted by yellow. U: uracil; A: adenine; G: guanine; C: cytosine.

TABLE 1 Sequences of miR-145 and its predicted target site on ARF6 mRNA.

RNA	Sequences
Mature miR-145	GUCCAGUUUUCCCAGGAAUCCCU
Predicted miRNA target site	AAGUGACUUUUGGGCAAAACUGGAA
MiRNA-mRNA duplex	AAGUGACUUUUGGGCAAAACUGGA AGUCCAGUUUUCCCAGGAAUCCCU

value is 1.00. The sequences from Figure 2 are shown in Table 1. Next, the secondary structures of all RNAs were predicted by using RNAfold. The resulting dot-bracket notations (Table 2) were inputted into simRNAweb to predict the tertiary structure of the RNA molecules. The 2D and 3D structures of the RNAs were shown in Figure 3.

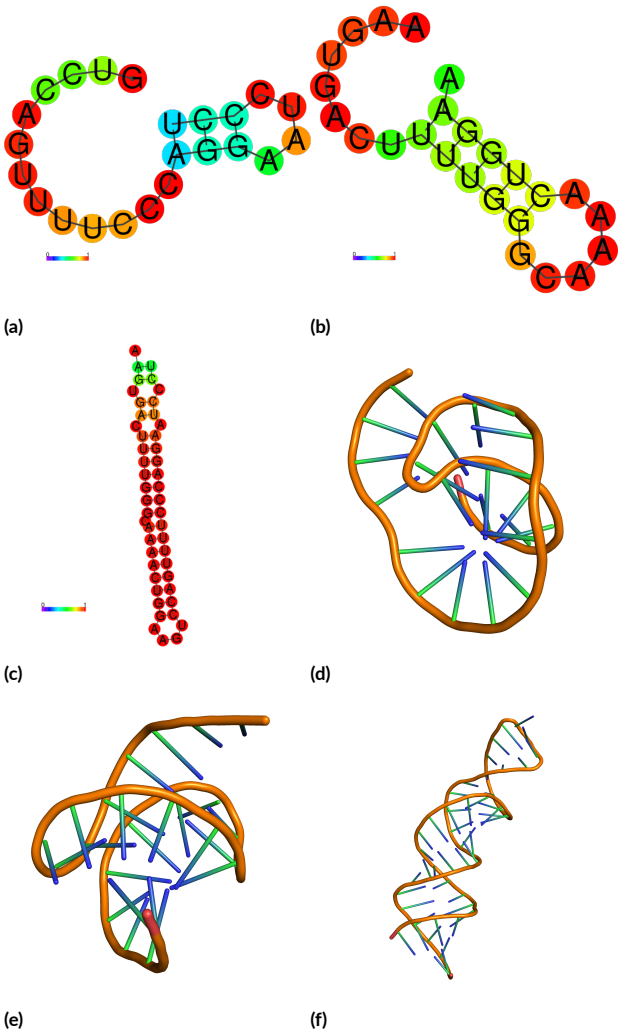

FIGURE 3 Secondary (a-c) and tertiary structures (d-f) of RNA molecules. (a,d) miR-145; (b,e) miRNA-target site of ARF6; (c,f) miRNA-mRNA duplex. The colors of secondary structures denoted the conserved region concerning the structure based on the base-pair probability parameter, from 0 (blue) to 1 (red).

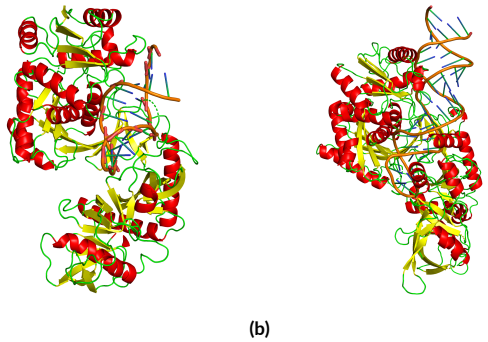

FIGURE 4 Docking result between a. miR-145 and b. miRNA-mRNA duplex with AGO protein. The visualization was done by using PyMOL 2.3.0.

3.2. Molecular docking and dynamics

We did two docking simulations: miR-145 & AGO protein and miRNA-mRNA duplex & AGO by using PatchDock Server. The best-scored model with negative thermodynamic value (Figure 4) was retrieved, with the statistical result shown in Table 3. Also, the docking result of AGO protein with its native ligand is showed in Table 3. The docking between miRNA and AGO protein shows a favorable interaction, denoted by the negative value of ACE (-532.40 kcal/mol) and supported by 18 inter-molecular hydrogen bonds (Table 4a). This also applies to the docking between miRNA-mRNA duplex and AGO protein (-84.58 kcal/mol) with 70 inter-molecular hydrogen bonds and 14 inter-molecular hydrophobic interactions (Table 4b

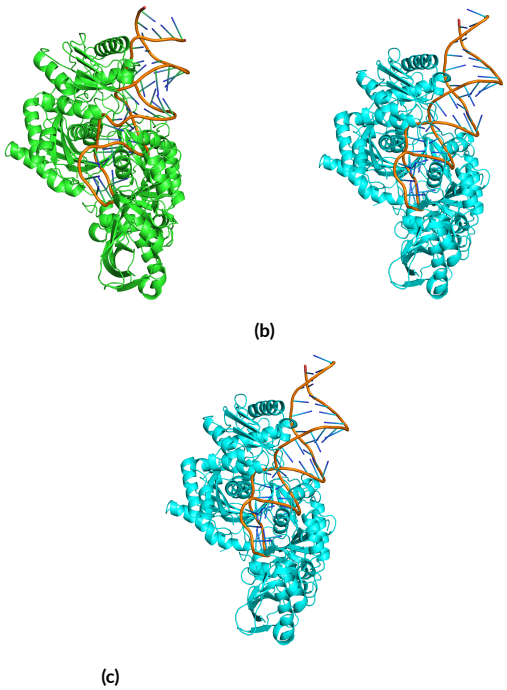

FIGURE 5 Molecular dynamics of mir-145 and second target site of 3'UTR of ARF6 mRNA. a. The first frame (initial molecule); b. Last frame; c. First and last frames. This shows the clear conformational difference between the initial and last states of the molecule. The visualization was done by using PyMOL 2.3.0.

TABLE 2 Secondary structure of RNA molecules.

RNA	Dot-bracket Notation	Minimum Free Energy (kcal/mol)
Mature miR-145	.....(((....)))	-1.10
Predicted miRNA target site	.....(((((.....))))).	-1.20
MiRNA-mRNA duplex	.((.((.(((((((.(((((((....)))))))))))))))).)).))	-19.80

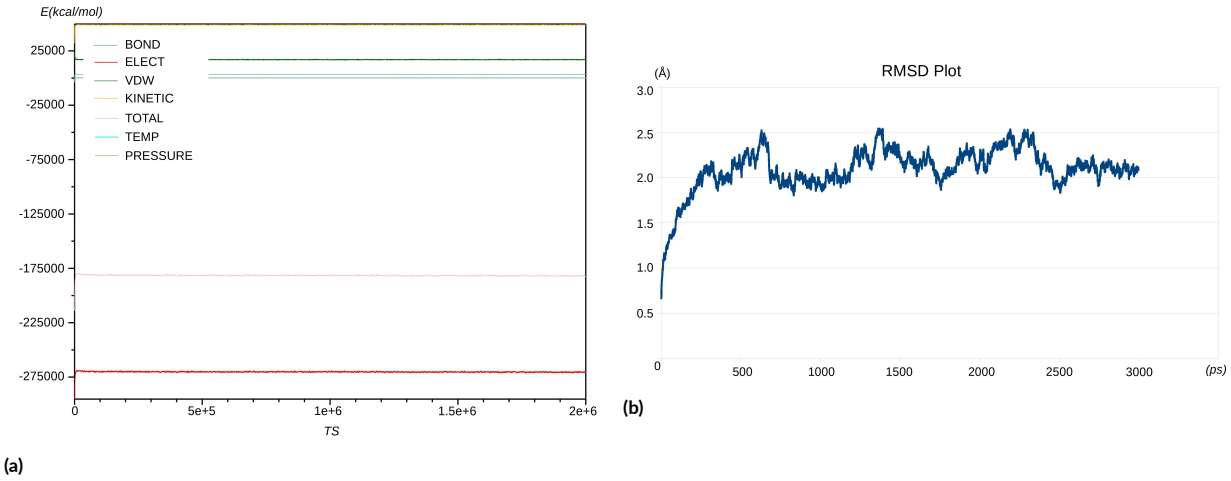

FIGURE 6 Time series of free energy (A) and RMSD plot (B) of the molecular dynamics simulation with 3,300 ps. The x and y-axis respectively denoted: a. time and energy (kcal/mol); b. time (ps) and energy (Å).

TABLE 3 Docking scores between miRNA-mRNA duplex and the native ligand (miR-20a) with AGO protein.

Molecule	Score	Area	ACE*	Transformation
miR-145-AGO	17,016	2,292.10	-532.40	-1.28 -1.43 -0.41 32.93 -11.56 43.87
RNA Duplex-AGO	16,712	4,608.80	-84.58	0.38 0.28 -3.06 49.82 70.46 58.33
Native ligand-AGO	18,842	2,488.50	-235.80	0.03 -0.22 -0.09 -14.89 6.62 8.00

*ACE: Atomic Contact Energy

and Table 5). Further molecular dynamics of the molecule is shown in Figure 5, as well as the free energy and RMSD plot of the protein backbone in Figure 6.

As shown in Figure 6a, the dynamics of conformational energy (i.e. bond), non-bond energy (i.e. vdW, electrostatic), and other energies (i.e. kinetic, total, temperature, pressure) of the molecule are stable after a short initial fluctuation. However, the RMSD of the molecule might not have reached equilibrium yet (Figure 6b): it still fluctuates in the range of 2.0 - 2.5Å until the end of the simulation. The previous study showed that wild-type miRNA-mRNA heteroduplex and AGO complexes stabilized at 1.5Å with larger fluctuations when the number of mismatches increased (Xia et al. 2013). As the interaction between miR-145, 3' UTR of ARF6 mRNA, and AGO was not included in the study (Xia et al. 2013), the equilibrium point might be higher. To better evaluate the energy-minimized state, the simulation should be done in a better computer to accommodate a longer time duration.

3.3. Discussion

According to Table 2, MFE of miR-145 and ARF6 mRNA duplex is -19.80 kcal/mol, which is generally lower than the previous study that comprised of 31 miRNA-mRNA interactions (Rath et al. 2016). Further docking analysis shows that there is favorable interaction between AGO-2 protein and miR-145. Interestingly, it has a lower ACE (-532.40 kcal/mol) than the native ligand of the protein (miR-20a, -235.780 kcal/mol). This might due to the structural similarity between miR-20a and miR-145. On the other hand, miR-regulated ARF6 and AGO have an ACE of -84.58 kcal/mol. This value is higher than the native ligand of the protein (miR-20a, -235.780 kcal/mol) as the protein conformation would best fit its natural ligand, as well as several siRNAs and miRNAs (Kandeel and Kitade 2013; Rath et al. 2016). Nevertheless, there are 70 hydrogen bonds and 14 hydrophobic interactions between the two molecules which stabilize the complex.

ARF6 has been found to promote the development of several types of cancer, for instance, breast cancer (Li et al. 2017). Moreover, several inhibitors have been found to suppress the activity of ARF6, resulting in the suppression of cancer invasion and/or metastasis (Li et al. 2017); this includes ARF6 small interfering RNA (siRNA) (Xu et al. 2015) and miR-145 (Eades et al. 2015). This idea was further supported by Ye et al. (2018), showing the inhibition of breast cancer development by overexpression of miR-145. Another study confirmed the low level of miR-145 expression among breast cancer patients with different onset of age, ranging from very young (<35 years old) until postmenopausal (>50 years old) patients (Tsai et al. 2018).

TABLE 4 Intermolecular hydrogen bonds position in: a. AGO protein sequence and miR-145, as well as b. AGO protein sequence and miRNA-mRNA duplex. Interaction format was written as protein receptor*-location: nucleic acid ligand**-location.

a. AGO protein - miR-145					
91:C11	A278:C17	H445:G3	N449:U4	R615:G8	F647:U20
L267:U14	R444:C22	H445:G3	H607:A19	R615:G8	R651:G6
E268:G13	R444:U23	H445:G21	H607:A19	S645:U4	R651:G7

b. AGO protein - miRNA-mRNA duplex						
R196:C29	R351:G22	D358:A16	R438:A6	N551:C37	H634:A24	Q757:U35
R196:A30	C352:G22	D358:C15	Q473:G5	R554:A39	R635:G22	T759:U33
Y225:G23	I353:C29	D358:C15	K476:G5	R554:A39	D669:A19	R761:U33
T259:G26	K354:G23	T361:C15	K476:U4	Q558:C7	Q708:U21	R761:U32
K260:U27	K354:G23	S362:C15	D480:G5	Q558:C7	K709:U33	R792:A17
K263:A24	K354:C29	R366:G14	K550:G13	S561:C7	R710:C20	R795:U35
L265:A25	K355:C29	T368:U33	K550:G13	N562:C37	R710:U21	A803:A19
R280:A24	K355:A30	D436:C7	K550:C38	D597:C20	R710:G31	Y804:U34
R351:G22	L356:A30	D436:C7	N551:C37	P602:C28	R714:U32	F811:A18
R351:G23	D358:A16	R438:A6	N551:C37	P602:G23	K726:U10	Y815:A16

*Amino acid = R: arginine; E: glutamic acid; Y: tyrosine; T: threonine; K: lysine; L: leucine; C: cysteine; I: isoleucine; D: aspartic acid; S: serine; Q: glutamine; N: asparagine; P: proline; H: histidine; A: alanine; F: phenylalanine.
**U: uracil; A: adenine; G: guanine; C: cytosine

Besides, the dependency of miR-145 suppression activity on AGO protein in breast cancer cells had recently been assessed (Bellissimo et al. 2019).

This study elucidates the regulation of ARF6 by miR-145 by the assistance of AGO protein based on in silico approach. The molecular docking shows a strong interaction between AGO and miR-145. In addition to negative value of MFE, the presence of hydrophobic aliphatic amino acids, such as alanine and leucine, provides structural stability between the molecules, while aromatic amino acids, such as histidine and phenylalanine, further support the complex stability. Furthermore, the interaction between AGO and the RNA duplex is also supported by strong hydrophobic amino acids, namely leucine, isoleucine, alanine, and phenylalanine. Further molecular dynamics affirms this stability, with stable dynamics and constant RMSD energy between 2.0–2.5 Å. However, there were several limitations that we encountered due to the unavailability of (i) reliable 3D structures of RNAs, (ii) RNA-specific molecular docking and dynamics software, and (iii) high-performance computer (HPC). As a result, the procedure was mostly done by using open-source online software, while the rest was simulated with limited computational power. Nevertheless, these results affirm the feasibility of molecular inhibition of ARF6 by miR-145 with the assistance of AGO protein. In this end, it is also emphasized that the high power GPU-based workstation with high specification of RAM and HDD is sufficient to conduct the whole computational process. This condition is mainly assisted by the availability of the High-resolution GPU in our workstation.

TABLE 5 List of hydrophobic interactions between the AGO protein receptor and the nucleic acid ligand.

Receptor Number	Receptor Type*	Ligand Number	Ligand Type**	Distance
260	Lys	27	U	3.90
263	Lys	25	A	3.72
353	Ile	23	G	0.71
354	Lys	29	C	3.78
355	Lys	29	C	2.88
355	Lys	29	C	2.31
362	Ser	15	C	2.55
436	Asp	7	C	3.99
557	Pro	7	C	3.40
601	Pro	28	C	3.96
602	Pro	28	C	3.44
608	Lys	28	C	3.80
804	Tyr	18	A	3.99
808	Leu	18	A	3.10

*Lys: lysine; Ile: isoleucine; Ser: serine; Asp: artic acid; Pro: proline; Tyr: tyrosine; Leu: leucine
**U: uracil; A: adenine; G: guanine; C: cytosine.

4. Conclusions

This study shows that there is a strong, favorable interaction between miR145, 3' UTR of ARF6 mRNA, and AGO protein computationally, affirming results from the previous studies. Future studies should incorporate the interaction between ARF6 mRNA and lincRNA-RoR, also, to complete the RISC molecule, to mimic their interactions in the real environment. The resulting binding affinity and stability of the molecules should be incorporated in further drug development to create a universal drug that mimics the activity of miR-145 in controlling ARF6 expression.

Acknowledgments

The authors would like to thank to Institute for Research and Community Services of Indonesia International Institute for Life Sciences (i3l) for their heartfelt support. Thanks goes to Direktorat Riset dan Pengabdian Masyarakat, Direktorat Jenderal Penguatan Riset dan Pengembangan Kementerian Riset, Teknologi dan Pendidikan Tinggi Republik Indonesia for providing Hibah Penelitian Berbasis Kompetensi DIKTI/KOPERTIS III 2018 No. 049/KM/PNT/2018 and Hibah Penelitian Dasar DIKTI No.T/140/E3/RA.00/2019. Thanks also go to the NVIDIA Corporation for providing Titan XP GPU with NVIDIA Academic Grant.

Authors' contributions

JI conducted the computational analysis and prepared the manuscript. AAP and RN supervised the study and manuscript writing.

Competing interests

The authors declare no competing interest.

References

Ahirwar R, Nahar S, Aggarwal S, Ramachandran S, Maiti S, Nahar P. 2016. In silico selection of an aptamer to estrogen receptor alpha using computational docking employing estrogen response elements as aptamer-alike molecules. Sci Rep. 6. doi:10.1038/srep21285.

Bellissimo T, Tito C, Ganci F, Sacconi A, Masciarelli S, Di Martino G, Porta N, Cirenza M, Sorci M, De Angelis L, et al. 2019. Argonaute 2 drives miR-145-5p-dependent gene expression program in breast cancer cells. Cell Death Dis. 10(1). doi:10.1038/s41419-018-1267-5.

Betel D, Wilson M, Gabow A, Marks DS, Sander C. 2008. The microRNA.org resource: Targets and expression. Nucleic Acids Res. 36(SUPPL. 1):D149–D153. doi:10.1093/nar/gkm995.

Boniecki MJ, Lach G, Dawson WK, Tomala K, Lukasz P, Soltysinski T, Rother KM, Bujnicki JM. 2015. SimRNA: a coarse-grained method for RNA folding simulations and 3D structure prediction. Nucleic Acids Res. 44(7):e63. doi:10.1093/nar/gkv1479.

Chou CH, Shrestha S, Yang CD, Chang NW, Lin YL, Liao KW, Huang WC, Sun TH, Tu SJ, Lee WH, et al. 2018. MiRTarBase update 2018: A resource for experimentally validated microRNA-target interactions. Nucleic Acids Res. 46(D1):D296–D302. doi:10.1093/nar/gkx1067.

Das RP, Konkimalla VB, Rath SN, Hansa J, Jagdeb M. 2015. Elucidation of the Molecular Interaction between miRNAs and the HOXA9 Gene, Involved in Acute Myeloid Leukemia, by the Assistance of Argonaute Protein through a Computational Approach. Genomics Inform. 13(2):45. doi:10.5808/gi.2015.13.2.45.

Djuranovic S, Nahvi A, Green R. 2011. A parsimonious model for gene regulation by miRNAs. Science 331(6017):550–553. doi:10.1126/science.1191138.

Duhovny D, Nussinov R, Wolfson HJ. 2002. Efficient unbound docking of rigid molecules. In: R Guigó, D Gusfield, editors, Algorithms in Bioinformatics. WABI 2002. Lecture Notes in Computer Science, volume 2452. Berlin, Heidelberg: Springer. p. 185–200. doi:10.1007/3-540-45784-4_14.

Eades G, Wolfson B, Zhang Y, Li Q, Yao Y, Zhou Q. 2015. LincRNA-RoR and miR-145 regulate invasion in triple-negative breast cancer via targeting Arf6. Mol Cancer Res. 13(2):330–338. doi:10.1158/1541-7786.MCR-14-0251.

Hashimoto S, Onodera Y, Hashimoto A, Tanaka M, Hamaguchi M, Yamada A, Sabe H. 2004. Requirement for Arf6 in breast cancer invasive activities. Proc Natl Acad Sci USA 101(17):6647–6652. doi:10.1073/pnas.0401753101.

Humphrey W, Dalke A, Schulten K. 1996. VMD: Visual Molecular Dynamics. J Mol Graph. 14(1):33–38. doi:10.1016/0263-7855(96)00018-5.

Janiszewska M, Primi MC, Izard T. 2020. Cell adhesion in cancer: Beyond the migration of single cells. J Biol Chem. 295(8):2495–2505. doi:10.1074/jbc.REV119.007759.

Kandeel M, Kitade Y. 2013. Computational Analysis of siRNA Recognition by the Ago2 PAZ Domain and Identification of the Determinants of RNA-Induced Gene Silencing. PLoS ONE 8(2):e57140. doi:10.1371/journal.pone.0057140.

Li J, Kim TH, Nutiu R, Ray D, Hughes TR, Zhang Z. 2014. Identifying mRNA sequence elements for target recognition by human Argonaute proteins. Genome Res. 24(5):775–785. doi:10.1101/gr.162230.113.

Li R, Peng C, Zhang X, Wu Y, Pan S, Xiao Y. 2017. Roles of Arf6 in cancer cell invasion, metastasis and proliferation. Life Sci. 182. doi:10.1016/j.lfs.2017.06.008.

Li R, Shen Q, Wu N, He M, Liu N, Huang J, Lu B, Yao Q, Yang Y, Hu R. 2018. MiR-145 improves macrophage-mediated inflammation through targeting Arf6. Endocrine 60(1):73–82. doi:10.1007/s12020-018-1521-8.

Liu H, Lei C, He Q, Pan Z, Xiao D, Tao Y. 2018. Nuclear functions of mammalian MicroRNAs in gene regulation, immunity and cancer. Mol Cancer 17(1):1–14. doi:10.1186/s12943-018-0765-5.

Lorenz R, Bernhart SH, Höner zu Siederdissen C, Tafer H, Flamm C, Stadler PF, Hofacker IL. 2011. ViennaRNA Package 2.0. Algorithms Mol Biol. 6(1). doi:10.1186/1748-7188-6-26.

Lorenz R, Luntzer D, Hofacker IL, Stadler PF, Wolfinger MT. 2016. SHAPE directed RNA folding. Bioinformatics 32(1):145–147. doi:10.1093/bioinformatics/btv523.

MacKerell Jr A. 2001. Atomistic Models and Force Fields. In: rO Becke, rA MacKerrel J, B Roux, M Watanabe, editors, Computational biochemistry and biophysics. New York: Marcel Dekker, Inc. p. 7–38.

Magnus M, Boniecki MJ, Dawson W, Bujnicki JM. 2016. SimRNAweb: a web server for RNA 3D structure modeling with optional restraints. Nucleic Acids Res. 44(W1):W315–W319. doi:10.1093/nar/gkw279.

Mrozik KM, Blaschuk OW, Cheong CM, Zannettino ACW, Vandyke K. 2018. N-cadherin in cancer metastasis, its emerging role in haematological malignancies and potential as a therapeutic target in cancer. BMC Cancer 18(1):1–16. doi:10.1186/s12885-018-4845-0.

Oh ES, Seiki M, Gotte M, Chung J. 2012. Cell adhesion in cancer. Int J Cell Biol. 2012:965618. doi:10.1155/2012/965618.

Pashaei E, Guzel E, Ozgurses ME, Demirel G, Aydin N, Ozen M. 2016. A Meta-Analysis : Identification of Common Mir-145 Target Genes that have Similar Behavior in Different GEO Datasets. PLoS ONE 11(9):e0161491. doi:10.1371/journal.pone.0161491.

Phillips JC, Braun R, Wang W, Gumbart J, Tajkhorshid E, Villa E, Chipot C, Skeel RD, Kalé L, Schulten K. 2005. Scalable molecular dynamics with NAMD. J Comput Chem. 26(16):1781–1802. doi:10.1002/jcc.20289.

Rath SN, Das D, Konkimalla VB, Pradhan SK. 2016. In Silico Study of miRNA Based Gene Regulation, Involved in Solid Cancer, by the Assistance of Argonaute Protein. Genomics Inform. 14(3):112–124. doi:10.5808/GI.2016.14.3.112.

Rehmsmeier M, Steffen P, Hochsmann M, Giegerich R. 2004. Fast and effective prediction of microRNA/target duplexes. RNA 10(10):1507–1517. doi:10.1261/rna.5248604.

Sabe H. 2003. Requirement for Arf6 in Cell Adhesion, Migration, and Cancer Cell Invasion. J Biochem. 134(4):485–489. doi:10.1093/jb/mvg181.

Salentin S, Schreiber S, Haupt VJ, Adasme MF, Schroeder M. 2015. PLIP: Fully automated protein-ligand interaction profiler. Nucleic Acids Res. 43(W1):W443–W447. doi:10.1093/nar/gkv315.

Schneidman-Duhovny D, Inbar Y, Nussinov R, Wolfson HJ. 2005. PatchDock and SymmDock: Servers for rigid and symmetric docking. Nucleic Acids Res. 33(SUPPL. 2):W363–W367. doi:10.1093/nar/gki481.

Tsai HP, Huang SF, Li CF, Chien HT, Chen SC. 2018. Differential microRNA expression in breast cancer with different onset age. PLoS ONE 13(1):e0191195. doi:10.1371/journal.pone.0191195.

Xia Z, Huynh T, Ren P, Zhou R. 2013. Large Domain Motions in Ago Protein Controlled by the Guide DNA-Strand Seed Region Determine the Ago-DNA-mRNA Complex Recognition Process. PLoS ONE 8(1):1–11. doi:10.1371/journal.pone.0054620.

Xu R, Zhang Y, Gu L, Zheng J, Cui J, Dong J, Du J. 2015. Arf6 regulates EGF-induced internalization of E -cadherin in breast cancer cells. Cancer Cell Int. 15(1). doi:10.1186/s12935-015-0159-3.

Xu WX, Liu Z, Deng F, Wang DD, Li XW, Tian T, Zhang J, Tang JH. 2019. MiR-145: a potential biomarker of cancer migration and invasion. Am J Transl Res. 11(11):6739–6753.

Ye P, Shi Y, An N, Zhou Q, Guo J, Long X. 2018. Biomedicine & Pharmacotherapy miR-145 overexpression triggers alteration of the whole transcriptome and inhibits breast cancer development. Biomed Pharmacother. 100:72–82. doi:10.1016/j.biopha.2018.01.167.

Zeinali T, Mansoori B, Mohammadi A, Baradaran B. 2019. Regulatory mechanisms of miR-145 expression and the importance of its function in cancer metastasis. Biomed Pharmacother. 109:195–207. doi:10.1016/j.biopha.2018.10.037.

Zhang R, Jing Y, Zhang H, Niu Y, Liu C, Wang J, Zen K, Zhang CY, Li D. 2018. Comprehensive Evolutionary Analysis of the Major RNA-Induced Silencing Complex Members. Sci Rep. 8(1):1–7. doi:10.1038/s41598-018-32635-4.

Zhang Y. 2013. RNA-induced Silencing Complex (RISC). In: W Dubitzky, O Wolkenhauer, KH Cho, H Yokota, editors, Encyclopedia of Systems Biology. New York: Springer New York. p. 1876. doi:10.1007/978-1-4419-9863-7_329.

Zhang Y, Verbeek FJ. 2010. Comparison and integration of target prediction algorithms for microRNA studies. J Integr Bioinform. 7(3):127. doi:10.1515/jib-2010-127.